Formation of star-like conjugated polymer films via electrooxidation of tris(4-carbazolylphenyl)amine and carbazole

Sophie Lakard [a], Anne-Félicie Lamic-Humblot [a], Vincent Humblot [b], Boris Lakard [a,*]

[a] Université Marie et Louis Pasteur, Institut UTINAM (UMR CNRS 6213), F-25000 Besançon, France

[b] Université Marie et Louis Pasteur, CNRS, Institut FEMTO-ST (UMR 6174), F-25000 Besançon, France

ABSTRACT

Tris(4-carbazoyl-9-ylphenyl)amine (TCA), owing to its conjugated and star-shaped structure, is a promising precursor for the formation of microporous conductive polymer films via electrochemical polymerization. However, the direct electrooxidation of TCA is challenging. To overcome this limitation, carbazole (Cz) was added to the acetonitrile electrolyte, enabling electropolymerization and film formation. Different feed ratios of TCA and Cz can be used to prepare polymer films and to study the impact of carbazole incorporation on the physicochemical properties of the electrodeposited materials. Thus, it is shown here that increasing the carbazole content facilitates the polymerization reaction and enhances the electroactivity of the resulting films, as evi- denced by higher capacitance and lower charge-transfer resistance. Based on these results, a mechanism for the electrochemical polymerization is proposed.

Introduction

Conducting polymers have attracted considerable attention because they combine electrical conductivity with the flexibility and process- ability of organic materials. These features make them suitable for ap- plications in organic electronics [1,2], energy storage [3,4], and adsorption or sensing of chemical species [5,6]. Among them, Conju- gated Microporous Polymers (CMPs) are a class of three-dimensional semiconducting organic polymers that integrate π-conjugation with intrinsic microporosity. Their rigid aromatic backbones ensure extended conjugation and favourable electronic properties for applications in energy storage or organic electronics, while their porous structure pro- vides high surface areas and enhanced adsorption capacity. The first CMP was reported in 2007 by Cooper et al., who synthesised a poly (aryleneethynylene) network via Sonogashira-Hagihara cross-coupling between alkynyl arene and halogenated aromatics [7]. Since then, numerous CMPs have been developed using various coupling strategies, including: Sonogashira-Hagihara [8,9], Suzuki-Miyaura [10,11], and Yamamoto reactions [12,13]. Owing to their tunable structures, CMPs have been explored in applications such as: photocatalysis [14,15], energy storage [16,17], and contaminant adsorption [18,19].

However, CMPs are typically obtained as insoluble powders due to their highly cross-linked structures, which limits their processabilityinto thin films. Electrochemical synthesis offers a promising alternative, as it enables the direct growth of polymer films on electrode surfaces through oxidative coupling of monomers. In this approach, radical species generated upon oxidation react to form a cross-linked structure. Piron et al. demonstrated this strategy by electropolymerizing a tetra- hedral bithiophenic-based monomer bearing four peripheral ethyl- enedioxythiophene units, leading to a three-dimensional π-conjugated network [20,21]. Using a similar approach, Gu et al. reported the elec- tropolymerization of tetrakis (4-(9H-carbazol-9-yl)phenyl)methane, which consists of a tetrahedral tetraphenylmethane core with four pe- ripheral electropolymerizable carbazole groups, yielding conductive polymer films applied as anode interlayers in polymer-light emitting diodes and photovoltaic cells [22]. They also investigated the electro- polymerization of 1,3,5-tris[4-(9-carbazolyl)phenyl]benzene, which consists of a 1,3,5-triphenylbenzene core with three peripheral N-substituted carbazole groups [23]. The resulting polymer films exhibited fluorescence properties suitable for sensing dopamine and metal ions [23]. The use of carbazole-based monomers was motivated by their high reactivity and relatively low oxidation potential, which facilitate film formation via anodic oxidation [24–26]. In addition, monomers with triangular or tetrahedral geometries promote the for- mation of three-dimensional, porous, and conjugated networks, as demonstrated by Gu *et al*. In view of literature results demonstrating the growth of star poly- mers from triangular or tetrahedral molecules bearing carbazole groups, the present work investigates tris(4-carbazoyl-9-ylphenyl)amine (TCA) as a monomer for the electrodeposition of conjugated polymer films. Indeed, TCA monomers have a star-shaped structure composed of a triphenylamine core with three peripheral electropolymerizable carba- zole groups (Fig. 1a and b). Polymer films were electrodeposited from solutions containing TCA alone or mixed with carbazole (Cz). Then, the physicochemical properties of the electrodeposited polymers were analyzed as a function of the amount of TCA and Cz molecules to evaluate the influence of the electrolyte solution. This study aims to assess the potential of TCA–carbazole polymer films for applications in organic electronics and energy storage.

Experimental details

Reagents

Tris(4-carbazoyl-9-ylphenyl)amine (>99%, Thermo Scientific), carbazole (>95%, Sigma-Aldrich), lithium

perchlorate (>95%, Sigma- Aldrich) and acetonitrile (>99.5%, Fisher Scientific) were used as received without further purification. Deionized water was obtained from a Synergy® Water Purification System and used in all experiments.

Electrochemistry

Instruments. All cyclic voltammetry and chronoamperometry exper- iments were performed using a Spelec instrument, from Metrohm, controlled by DropView software. Electrochemical impedance spec- troscopy and galvanostatic charge-discharge measurements were car- ried out with a SP-200 instrument, from Biologic, controlled by EC-Lab
software. Electrochemical experiments were carried out in a conven- tional three-electrode cell composed of a platinum wire (0.785 mm^2) or
a fluorine-doped tin oxide (FTO) substrate (R 80 Ω/square, 15 mm 30 mm) as the working electrode, a platinum plate (5 cm 5 cm 0.1 cm) as the counter-electrode, and a saturated calomel electrode (SCE) as the reference electrode.
Electrolytic solutions were prepared from TCA, Cz, or mixtures of both at different volume ratios (TCA75:Cz25, TCA50:Cz50, and TCA25: Cz75). For example, the TCA75:Cz25 electrolyte (10 mL) was obtained by mixing 7.5 mL of a 0.01 M TCA solution with 2.5 mL of a 0.01 M Cz solution, both containing 0.1 M $LiClO_4$ as supporting electrolyte.
Polymer films were *electrodeposited* either by cycling voltammetry (CV) on a platinum working electrode in a potential range of 0.0 to 1.5 V/SCE at 50 mV/s, or by chronoamperometry on a FTO electrode at a potential of 1.2 V/SCE for 10 min. The use of transparent FTO sub- strates facilitated visualization of the deposited films. Additional CVs were performed at different scan speeds (50, 100, 150, 200 and 250 mV/
s) in monomer-free electrolyte ($LiClO_4$ at 0.1 M) to assess whether the electrochemical response was diffusion-controlled. Post-polymerization CVs were also performed with the polymer-modified electrode in monomer-free solution (5 potential scans from 0.0 to 1. 5 V/SCE at 50 mV/s) to evaluate the electrochemical activity of the polymer films.
Electrochemical Impedance Spectroscopy (EIS) measurements were performed in monomer-free electrolyte over a frequency range from 100 kHz to 0.1 Hz, with 6 points per frequency decade. Spectra were recorded at 0.6 V/SCE (E_{dc}) with a modulation voltage of 50 mV (E_{ac}). Data were fitted using a combination of Randomize (5000 iterations) and Simplex method, with fitting stopped after 5000 iterations).
Galvanostatic Charge-Discharge (GCD) experiments were performed at current densities ranging from 0.2 to 1.0 mA/cm^2 within a potential window of 0.0 to 1.2 V/SCE, corresponding to the redox region of the electrodeposited films.

Characterization techniques

SEM microscopy. The surface morphology of the electrodeposited films was examined without prior metallization using a high-resolution Thermo Scientific Apreo 2 scanning electron microscope. Images were acquired with a beam accelerating voltage of 5 keV, a probe current of
0.1 nA, and a working distance of 10 mm.
The *XPS analyses* were performed using a Thermo Fisher (Thermo Fisher Scientific, Waltham, MA, USA) NEXSA G2 photoelectron spec- trometer, equipped with a standard monochromated AlKα source, operated at a 120 W electron beam power. The emission of photoelec-
trons from the sample was analyzed at a takeoff angle of 90° under ultra- high vacuum conditions of 10^{-9} mbar. Spectra acquisition was carried out with 150 eV pass energy for the survey scan (1 eV step) and 50 eV
pass energy for the C1s, O1s, N1s, F1s, S2p, and Sn3d (0.05 eV step). Binding energies (BEs) were calibrated against C 1 s aliphatic carbon bonds (C–C and C–H) binding energy at 284.8 eV, and element peak intensities were corrected according to Scofield factors [27]. The spectra were fitted using the Casa XPS v.2.3.15 software (Casa Software Ltd., Cardiff, UK) and applying a Gaussian/Lorentzian ratio equal to 70/30. The peak areas were determined after subtraction of a Shirley background.
Profilometry. A Dektak XT stylus profilometer from Brüker was used to measure the thickness of the electrodeposited films. Measurements were done over a scale length of 2000 μm at a scan speed of 70 μm/s, using a stylus with a radius of 12.5 μm. The average thickness was calculated from at least 3 measurements taken at different locations on each sample.
Results and discussion

Electrochemical oxidation of the monomers

The electrochemical oxidation of TCA was performed in an aceto- nitrile solution containing $LiClO_4$ within a potential window of 0.0 to +1.5 V/SCE using cyclic voltammetry (CV). During the first scan, a slight increase in current was observed above 0.9 V/SCE (Fig. 2a), corresponding to the oxidation of the carbazole units in the TCA struc- ture. However, the current remained low and did not increase upon successive cycles. At the end of the experiment, only a thin yellow film was visible on the electrode surface to the naked eye.

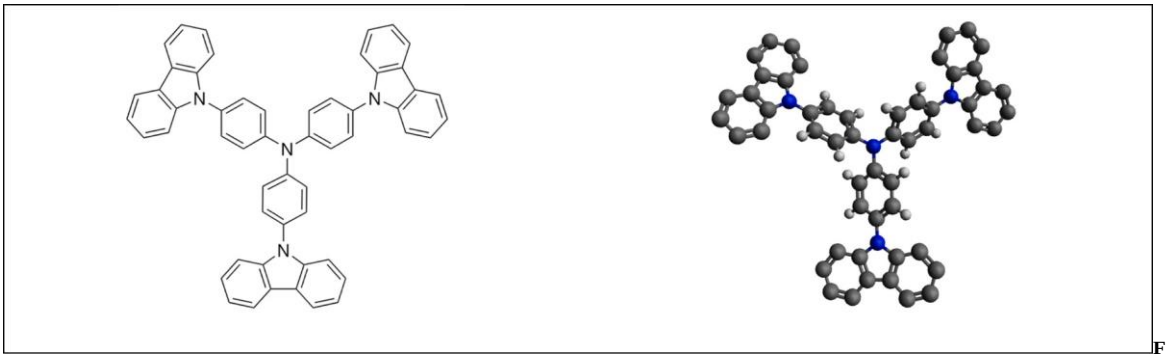

Fig. 1. Structure of tris(4-carbazoyl-9-ylphenyl)amine.

To promote the electrodeposition of conductive films, TCA, TCA:Cz mixtures were then prepared. Cz was introduced both to enhance TCA inacetonitrile and to provide additional electropolymerizable carbazole units. For all compositions, a well-defined anodic peak appeared be- tween 1.05 and 1.10 V/SCE from the first potential scan (Fig. 2b–d). This anodic peak was also present at 1.05 V/SCE for Cz alone (Fig. 2e), indicating that the signal arises from the oxidation of carbazole units in both Cz and TCA.

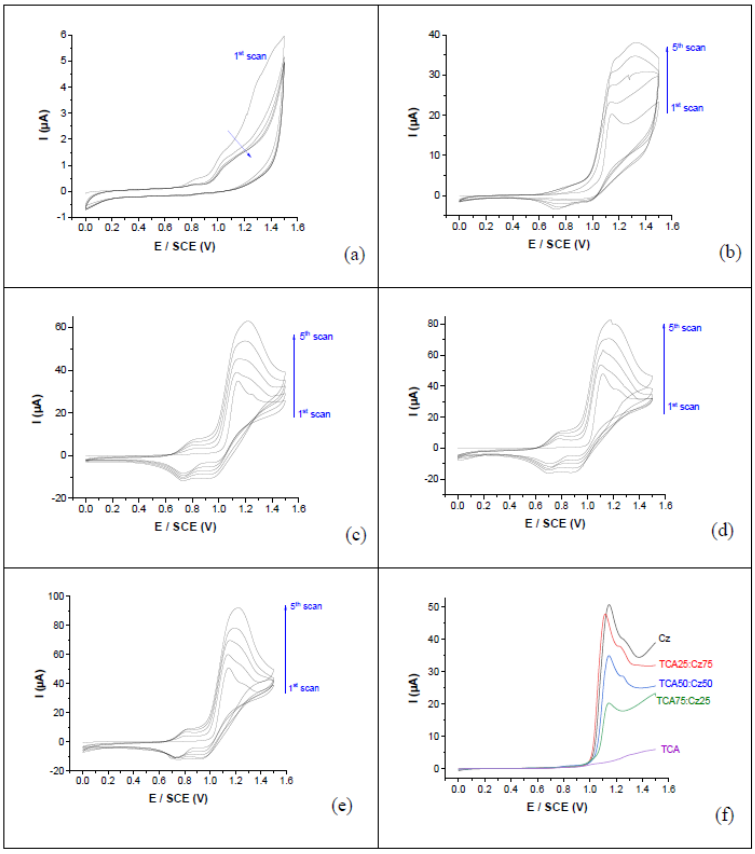

Fig. 2. Cyclic voltammograms obtained by oxidation of TCA (a), TCA75:Cz25 (b), TCA50:Cz50 (c), TCA25:Cz75 (d), and Cz (e) in an acetonitrile + 0.1 M $LiClO_4$ solution. Comparison of the first potential scan of the different electrolytes (f). WE: Pt, CE: Pt, RE: SCE. Scan rate: 50 mV/s.

Upon successive cycling, the intensity of the peak increased steadily, indicating the formation of a thick conductive film on the electrode surface. The resulting film was green and clearly visible to the naked eye. Moreover, the intensity of the peak increased from 20 to 47 μA as the Cz content rose from 25% to 75% (Fig. 2f), demonstrating that Cz promotes film formation and increased its conductivity. From the second scan, a reduction peak appeared at 1.05 V/SCE, which may be asso- ciated with the oxidation process of the carbazole units, while another pair of oxidation/reduction peaks emerged at 0.80 V/SCE and 0.70 V/SCE, corresponding to the oxidation/reduction of the growing poly- mer film.

Moreover, the shift in oxidation peak potentials from 0.90 to 1.05 V/SCE upon addition of Cz can be attributed to the contribution of free carbazole, which oxidizes at +1.05 V/SCE and dominates the electro- chemical response of the mixture. In addition, π–π interactions between carbazole units in TCA and Cz likely modify the electronic environment, making oxidation slightly less favorable. As a result, the observed peak corresponds to a combined response shifted toward the intrinsic oxida- tion potential of carbazole.

The influence of the scan rate on the cyclic voltammograms was investigated to determine the mode limiting the transport of the monomers at the platinum electrode. For that, the electrochemical oxidation of TCA, Cz, and TCA:Cz mixtures was carried out in acetoni- trile containing $LiClO_4$ at scan rates ranging from 50 to 250 mV/s (Fig. 3a–e). The intensity of the main anodic (1.25 V/SCE) and cathodic (1.15 V/SCE) peaks was plotted as a function of the square root of the scan rate (Fig. 3f). For all solutions containing Cz, the peak current (i_p) varied linearly with $v^{1/2}$, in agreement with the Randles- Sevcik equation (Eq. 1). This confirms that the electrochemical process is diffusion-controlled, indicating that the transport of electro- active species from the bulk solution to the electrode surface is the rate- limiting step, consistent with previous reports on carbazole derivatives [28,29]. In contrast, no linear relationship was observed for the solution containing only TCA molecules. These data were therefore excluded from Fig. 3f and Table 1.

$$i_p = 2.69 \times 10^5 n^{3/2} A C D^{1/2} v^{1/2} \quad (1)$$

Where i_p is the peak current, n the number of electrons transferred in unit reaction, A the electrode area, C the concentration, D the diffusion coefficient, and v the scan rate.

According to Randles-Sevcik equation, the diffusion coefficient, which quantifies the speed at which electroactive species can move through a solution due to concentration gradients, can be deduced from the slope of the linear relationship between i_p and $v^{1/2}$. As shown in Table 1, the slope of these linear fits increases with the Cz content in the solution, ranging varying from 4.36 to 13.06 μA/(V/s)$^{1/2}$ for the anodic peak and from 3.30 to 10.41 μA/(V/s)$^{1/2}$ for the cathodic peak. This behavior suggests that, in the presence of Cz, the oxidation involves freely diffusing species rather than surface-confined processes, and that electron transfer kinetics are sufficiently fast to maintain reversibility. The increase in slope with Cz content reflects a higher effective diffusion coefficient and/or a greater concentration of electroactive carbazole species, which enhances mass transport and contributes to the improved electrochemical response.

After that, polymer films were electrodeposited onto FTO substrates to be visualized more easily. All polymer films exhibited a dark green coloration, except for the polyTCA film, which appeared thinner and less intensely coloured (Table 1). The polymer films were also electro- deposited using chronoamperometry to evaluate the charge density associated with the polymerization reaction, providing insight into its efficiency. The highest charge density was measured for the polyCz film (6.45 mC/mm^2), whereas the lowest one was obtained for the polyTCA film (0.74 mC/mm^2). For mixed TCA:Cz systems, the charge density increased with the Cz content, rising from 3.85 mC/mm^2 for TCA75: Cz25 film to 5.41 mC/mm^2 for TCA25:Cz75 film. This trend confirms that higher Cz concentrations facilitate the polymerization process.

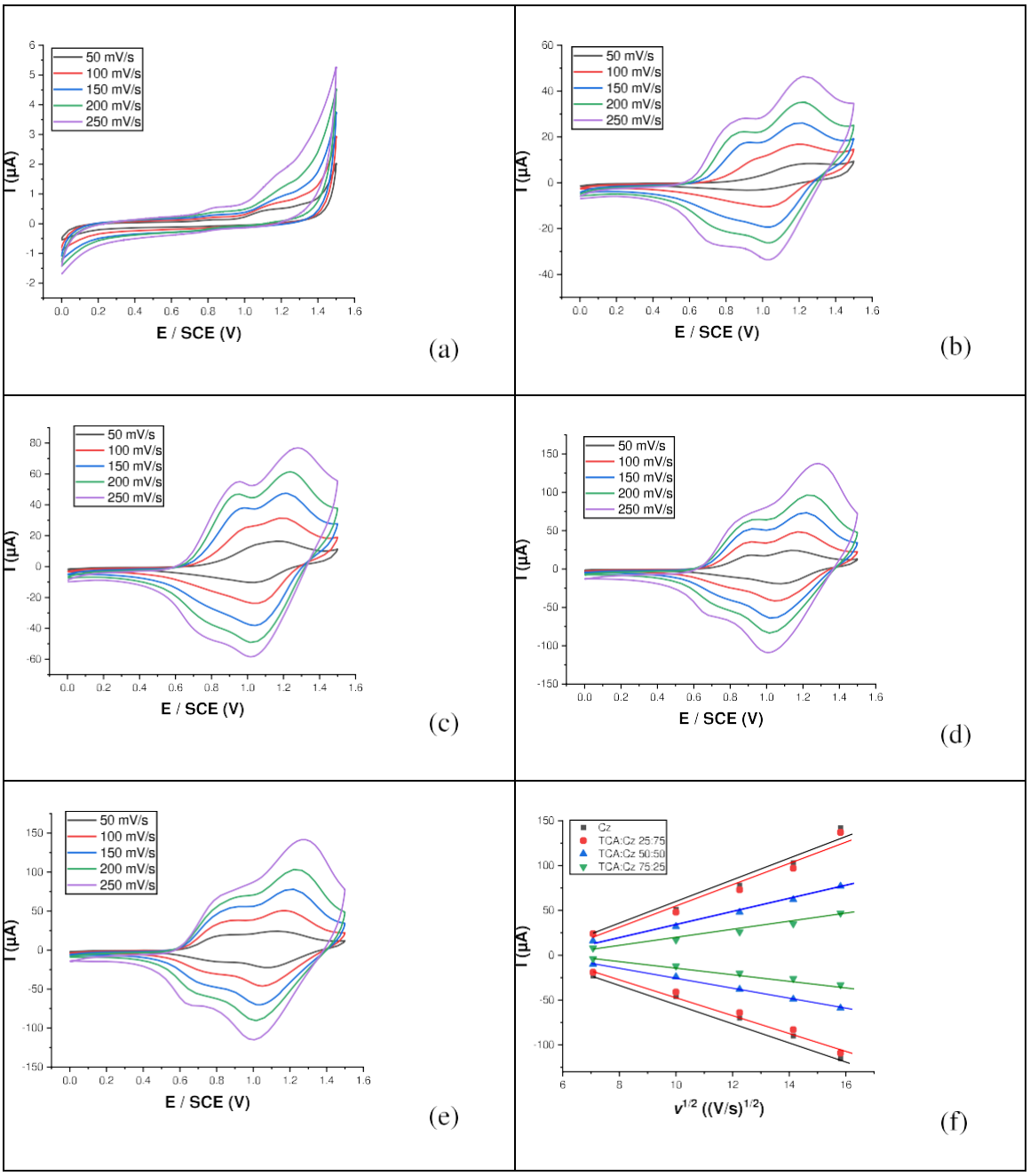

Fig. 3. Cyclic voltammograms obtained by oxidation of TCA (a), TCA75:Cz25 (b), TCA50:Cz50 (c), TCA25:Cz75 (d), and Cz (e) in an acetonitrile + 0.1 M $LiClO_4$ solution. Variation of the anodic and cathodic peak currents (5th scan) as a function of the square root of the scan rate (f). WE: Pt, CE: Pt, RE: SCE.

Morphology of the electrodeposited films

Scanning electron microscopy was used to investigate the morphology of the electrodeposited polymer films. The polyCz film, formed by oxidation of carbazole, consisted of randomly distributed globules on the surface of the FTO substrate (Fig. 4a) as already observed for other polymers obtained by electrodeposition of carbazoles [26,30]. Numerous cracks were also observed, reflecting the film's high stiffness as previously measured by AFM measurements of its Young's modulus [31,32]. The TCA25:Cz75 film displayed a very similar struc- ture made of globules but without cracks, indicating that the addition of TCA improves film uniformity (Fig. 4b). In contrast, the TCA50:Cz50 and TCA75:Cz25 films exhibited distinct structures. Indeed, the TCA50: Cz50 was dominated by needle-like features of varying sizes (Fig. 4c), while the TCA75:Cz25 film consisted of unevenly distributed aggregates rather than the typical polycarbazole globular morphology (Fig. 4d).

The globular morphology observed for polyCz and TCA25:Cz75 films provides a homogeneous and

interconnected structure that facilitates charge transport and ion diffusion, resulting in improved electroactivity, higher capacitance, and lower charge-transfer resistance, as shown in Section 3.4. In contrast, the presence of cracks in polyCz likely hinders charge transport despite its similar morphology. The crack-free globular structure of TCA25:Cz75 thus explains its superior performance. On the other hand, the needle-like morphology observed for TCA50:Cz50 and the aggregated structure of TCA75:Cz25 are expected to create less uniform and less conductive pathways, limiting efficient charge trans- port and electrolyte accessibility. This structural heterogeneity likely contributes to their lower electrochemical performance compared to Cz- rich films.

Electrolytic solution	TCA	TCA75: Cz25	TCA50: Cz50	TCA25: Cz75	Cz
Anodic slope ($\mu A/(V/s)^{1/2}$)	—	4.36	6.96	12.43	13.06
Cathodic slope ($\mu A/(V/s)^{1/2}$)	—	−3.30	−5.66	−10.12	−10.41
Picture					
Charge density (mC/mm^2)	0.74	3.85	5.05	5.41	6.45
Thickness (μm)	0.56	3.25	3.72	4.32	4.40

Table 1
Anodic and cathodic slopes of the i-$v^{1/2}$ curves, charge density deduced from i-t transients, thickness measured by profilometry, and picture of the electro- deposited films.

XPS analysis of the electrodeposited films

The theoretical carbon and nitrogen proportions in Cz and TCA molecules were calculated based on their chemical formulas (Table 2, Fig. 5). TCA contains a higher proportion of carbon and a lower pro- portion of nitrogen compared to Cz. The theoretical proportions for the TCA – Cz mixtures were also calculated from their initial compositions. XPS measurements were subsequently performed, allowing determina- tion of the atomic proportions in the electrodeposited films. As expected, the carbon content increases from 91.70% to 92.70% and the nitrogen content decreases from 8.30% to 7.30% as the Cz proportion is reduced from 100% to 50%. These results, together with the good agreement between theoretical and experimental proportions, demonstrate the presence of TCA in the polymer films. If the TCA75:Cz25 mixture does not follow this trend, this can be explained by the fact that TCA cannot polymerize alone, while its polymerization is possible but difficult when it is present as a minor component. As a result, the atomic distribution in this film may not be homogeneous, likely due to the insufficient amount of Cz.

Electrochemical reaction mechanism

As described by Ambrose and Nelson [33] and confirmed by others [31,33–35], the electrochemical oxidation and polymerization of carbazole-containing compounds follows an ECE (Electrochemical – Chemical – Electrochemical) mechanism (Fig. 6). The reaction begins with the oxidation of carbazole units at the electrode, generating radical cations that delocalize to the C_6 position. Coupling then occurs between two radical cations at the C_6-$C_{6'}$ positions, stabilizing the system, fol- lowed by deprotonation of C_6 and $C_{6'}$ to restore aromaticity of the benzene rings. The resulting dimer can undergo further oxidation and coupling, leading to polymer chain growth. In electrolytes containing only carbazole, this mechanism produces polycarbazole films. When both TCA and carbazole are present, multiple pathways occur: (i) chain growth around TCA molecules via oxidation and coupling of carbazole groups with other TCA units or free carbazole in solution, and (ii) pol- ycarbazole chain growth by coupling between free carbazole. Electro- chemical data suggest that carbazole facilitates TCA polymerization while also participating in cross-linked copolymer formation.

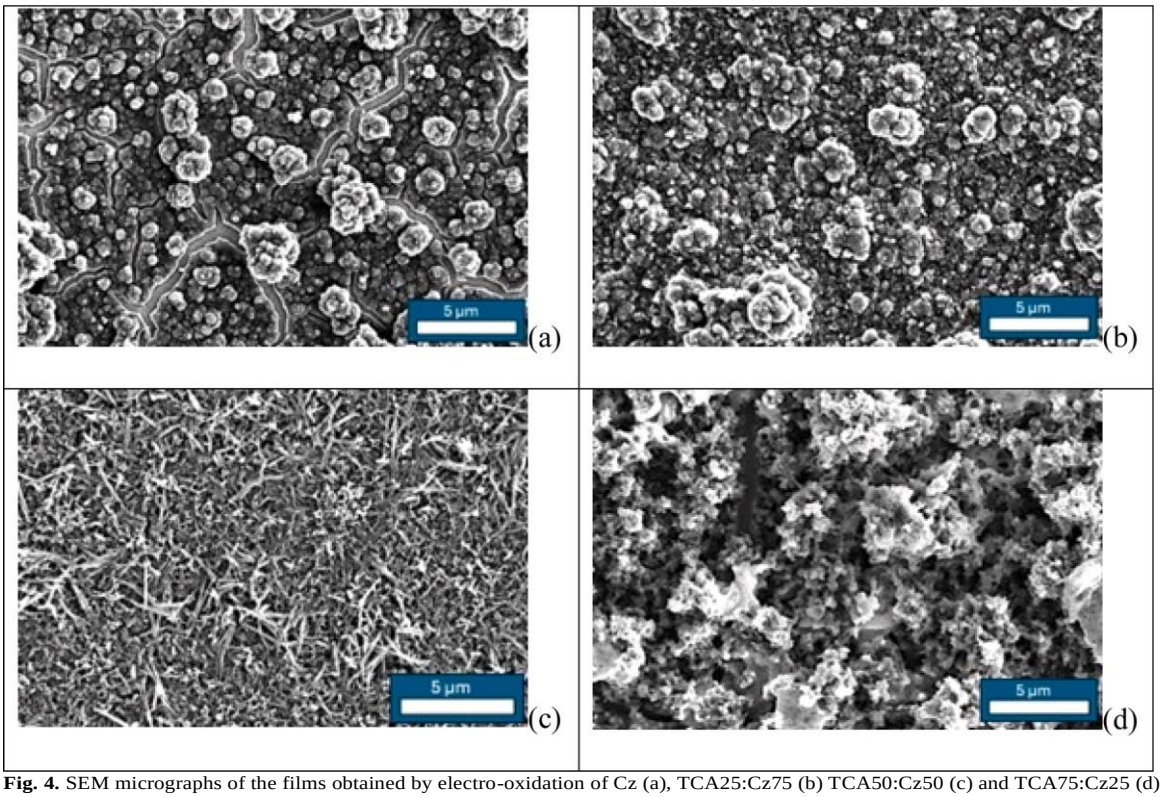

Fig. 4. SEM micrographs of the films obtained by electro-oxidation of Cz (a), TCA25:Cz75 (b) TCA50:Cz50 (c) and TCA75:Cz25 (d) in an acetonitrile + 0.1 M $LiClO_4$ solution.

Table 2 Theoretical and XPS experimental proportions of carbon and nitrogen atoms into the electrolytes and polymer films, respectively.

Electrolyte	%N theo	%C theo	Polymer	%N exp	%C exp
Cz	7.69	92.31	PolyCz	8.30	91.70
TCA25:Cz75	7.22	92.78	Poly(TCA25:Cz75)	7.60	92.40
TCA50:Cz50	7.04	92.96	Poly(TCA50:Cz50)	7.30	92.70
TCA75:Cz25	6.95	93.05	Poly(TCA75:Cz25)	7.80	92.20
TCA	6.90	93.10	PolyTCA	x	x

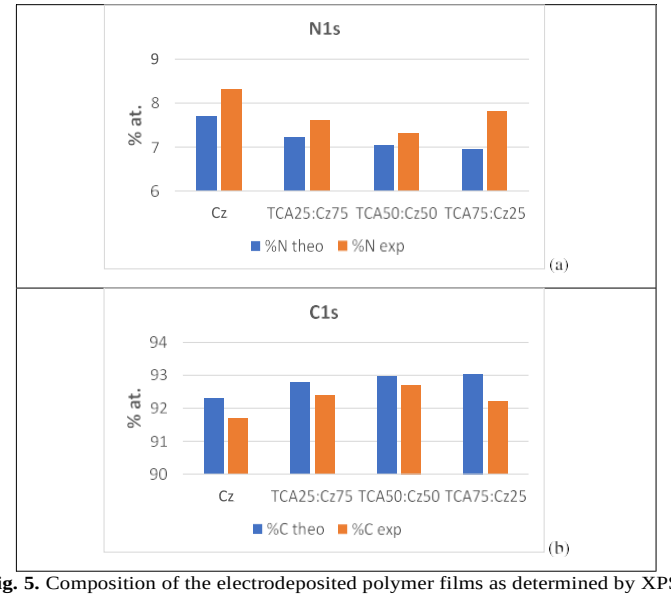

Fig. 5. Composition of the electrodeposited polymer films as determined by XPS analysis: (a) nitrogen content and (b) carbon content.

The resulting polymer films are therefore likely a mixture of polyCz, polyTCA and TCA–Cz copolymer. However, distinguishing these com- ponents spectroscopically is challenging, as carbazole and TCA share identical functional groups. Infrared spectra of the electrodeposited films were recorded but appeared very similar, preventing unambiguous identification of the individual polymer components.

Electrochemical properties of the electrodeposited films

Electrochemical activity measurements

To assess the electroactivity of the electrodeposited polymer films and their ability to mediate electron transfer with species in the elec- trolyte, post-polymerization CVs were carried out using polymer- modified Pt electrodes as the working electrode, and a monomer-free solution of acetonitrile / lithium perchlorate solution was used as the electrolyte.

Post-polymerization CVs of films electrodeposited from TCA50:Cz50, TCA25:Cz75Cz and Cz solutions exhibited both an oxidation and a reduction peak indicating a doping / dedoping process, although the anodic peak was significantly more pronounced than the cathodic one (Fig. 6b–d). In contrast, the TCA75:Cz25 film showed a very weak oxidation peak and no reduction peak, which is characteristic of a largely non-electroactive material (Fig. 6a). The decrease in electro- activity with increasing TCA content is consistent with the findings of Kimpel et al., who reported that 3,9-substituted carbazole units reduce electroactivity [36]. Fig. 6e compares the first cycle of these post-polymerisation CVs, showing oxidation peak currents of 25, 23, and 13 μA for Cz, TCA25:Cz75 and TCA50:Cz50, respectively, while the reduction peaks were all below 5 μA. In all cases, the intensity of the redox peaks decreased over cycles. These results indicate that only films prepared from solutions containing at least 50% Cz display sufficient electrochemical activity for applications requiring efficient electron transfer.

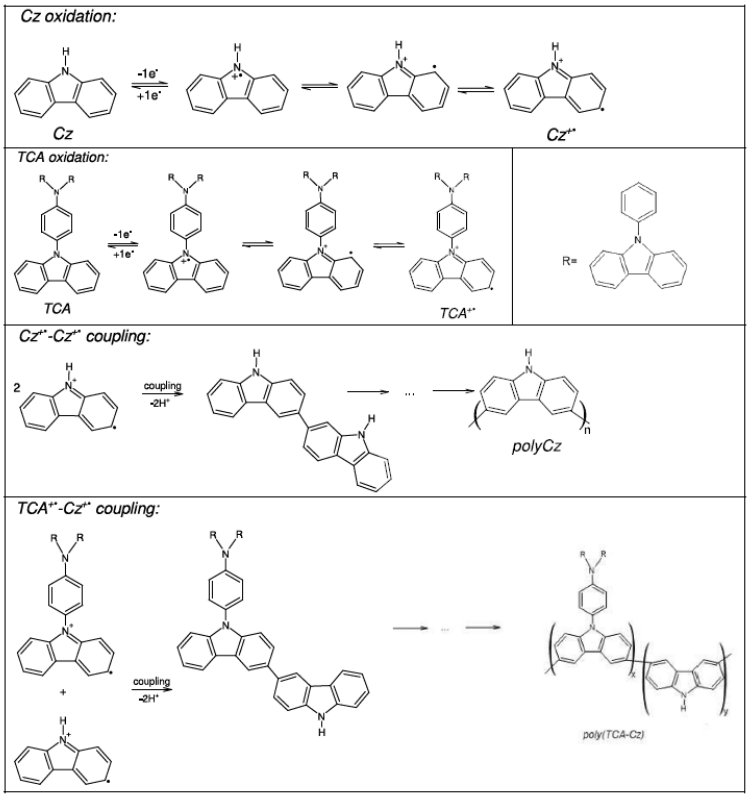

Fig. 6. Reaction mechanism for the electropolymerization of carbazole derivatives.

Galvanostatic charge-discharge

Galvanostatic charge – discharge (GCD) measurements of the elec- trodeposited polymer films were carried out at current densities ranging from 0.2 to 1.0 mA/cm^2 over a potential window of 0 to +1.2 V/SCE (Fig. 7a–d) to evaluate their capacitance. The GCD curves exhibited a triangular shape with slight asymmetry, indicating that the electro- deposited polymer films are pseudo-capacitive materials. Fig. 8 clearly shows that charge and discharge times decreased with increasing cur- rent density, indicating that the charge and discharge processes take place more rapidly at higher current, independent of the film composition.

To compare the electrochemical performance of the different polymer-modified electrodes, the discharge specific capacitance (C) was calculated from the galvanostatic potential–time transients using the following equation (Eq. 2) [37]: parallel combination of the charge-transfer resistance (R_{ct}) and a con- stant phase element (Q), both associated with Faradaic processes. The Nyquist plots (Fig. 9a) exhibited a quasi-perfect semicircular arc inter- secting the real axis at two points. The high-frequency intercept corre- sponds to the

solution resistance (R_s), while the low-frequency intercept gives the total resistance (R_s R_{ct}). The diameter of the semicircle decreased with increasing carbazole content, indicating a reduction in charge-transfer resistance and thus improved conductivity. This trend suggests that higher carbazole content promotes the formation of more extended conjugated polymer networks.

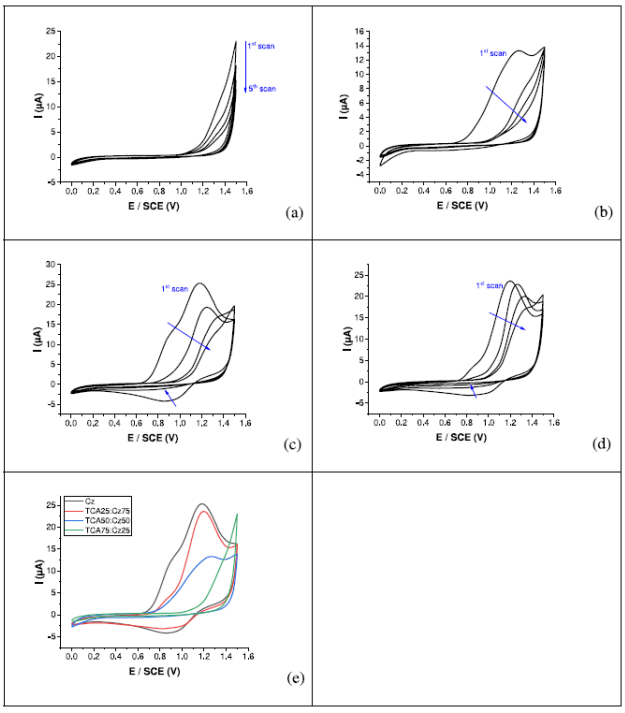

Fig. 7. Post-polymerization cyclic voltammograms obtained by oxidation of TCA75:Cz25 (a), TCA50:Cz50 (b), TCA25:Cz75 (c), and Cz (d) in an acetonitrile + 0.1 M $LiClO_4$ solution. Comparison of the first potential scan of the different electrodeposited films in monomer-free electrolytes (e). WE: Pt, CE: Pt, RE: SCE. Scan rate: 50 mV/s. The polymer films studied here were previously deposited by cyclic voltammetry using the same deposition conditions as in Fig. 2.

Fitting parameters (Table 3) were extracted from the application of the Randles equivalent circuit model to the experimental impedance spectra using EC-Lab software. The TCA75:Cz25 film exhibited the highest Rct (135,146 Ω), whereas the polyCz film showed the lowest value (65,000 Ω), indicating the most efficient charge-transfer interface. Variations in other fitting parameters were less significant. Differences in the solution resistance reflect changes in electrolyte composition, while the constant phase element remained relatively unchanged.

Bode plots deduced from EIS spectra were also analyzed to better visualize frequency-dependent behavior. The Bode magnitude plots confirmed that the polyCz film is the least resistive over the entire fre- quency range (Fig. 8b). In contrast, the phase Bode plot showed no significant differences between the films, providing limited additional insight (Fig. 8c).

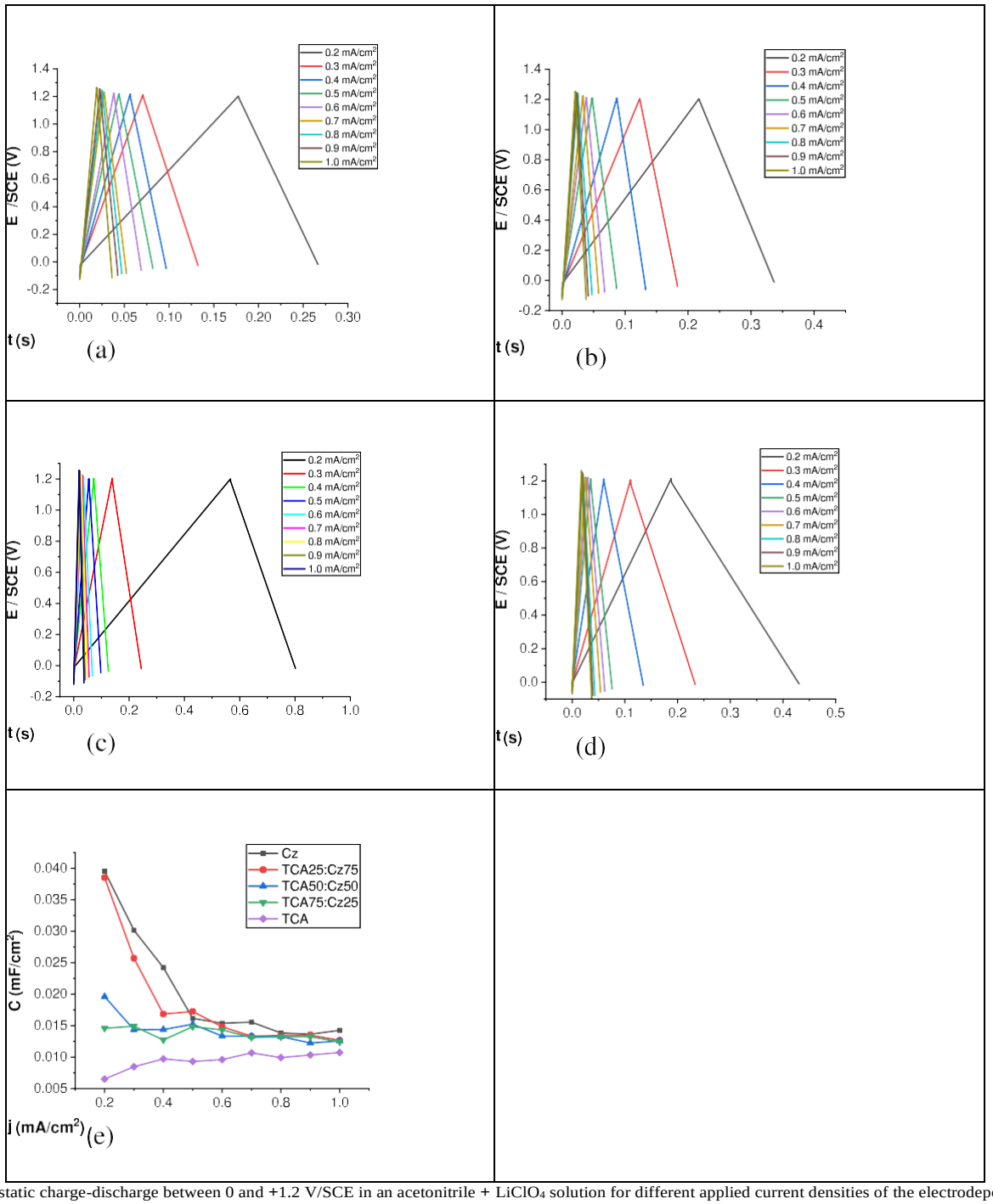

Fig. 8. Galvanostatic charge-discharge between 0 and +1.2 V/SCE in an acetonitrile + $LiClO_4$ solution for different applied current densities of the electrodeposited films obtained by oxidation of TCA75:Cz25 (a), TCA50:Cz50 (b), TCA25:Cz75 (c), and Cz (d) in an acetonitrile + 0.1 M $LiClO_4$ solution. Variation of capacitance as a function of current densities of the electrodeposited films (f). WE: Pt. The polymer films studied here were previously deposited by cyclic voltammetry using the same deposition conditions as in Fig. 2.

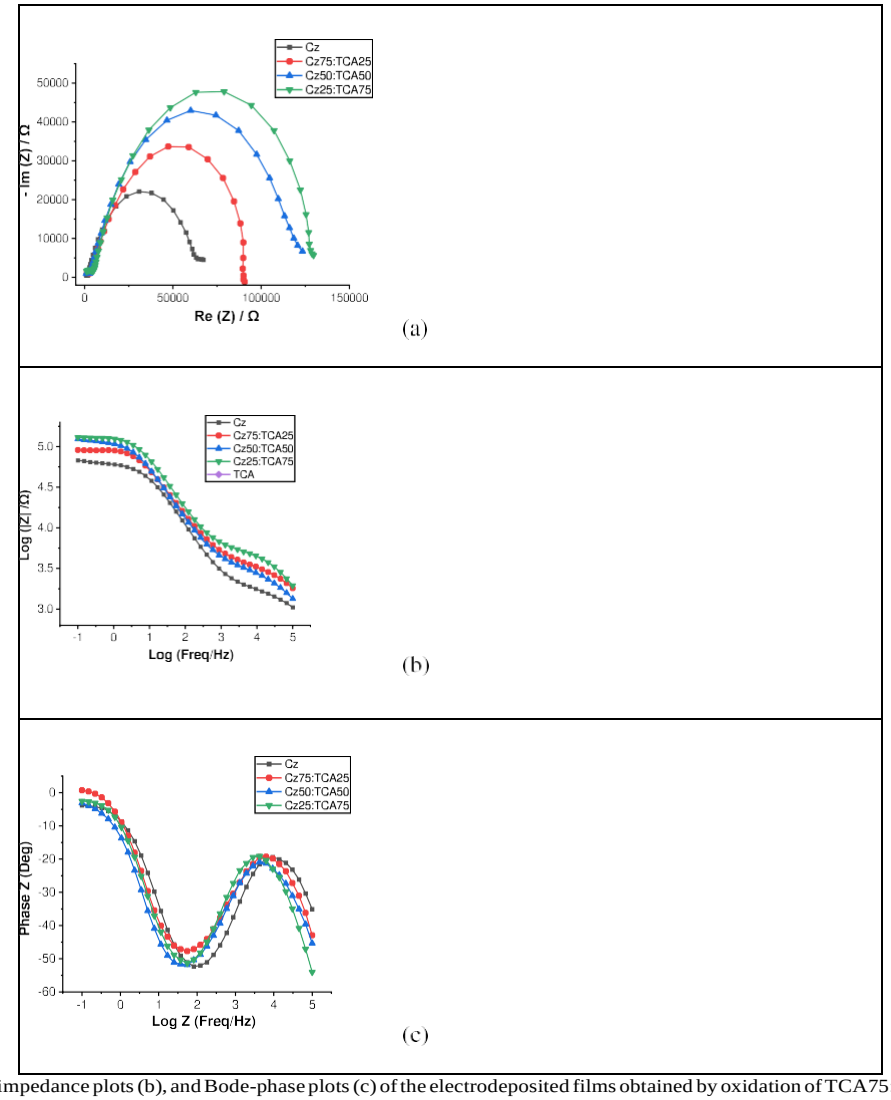

Fig. 9. Nyquist plots (a), Bode-impedance plots (b), and Bode-phase plots (c) of the electrodeposited films obtained by oxidation of TCA75:Cz25 (a), TCA50:Cz50 (b), TCA25:Cz75 (c), and Cz (d) in an acetonitrile + 0.1 M $LiClO_4$ solution. Initial potential E = +0.6 V/SCE. Highest Freq = 100 kHz, Lowest Freq = 0.1 Hz. WE: Pt. The polymer films studied here were previously deposited by cyclic voltammetry using the same deposition conditions as in Fig. 2.

Table 3
Values extracted from the application of a simple Randles equivalent circuit model to the impedance data for the different electrodeposited films (R_s: solu- tion resistance, Q: constant phase element, R_{ct}: charge transfer resistance).

Electrolyte	R_s (Ω)	Q (μF.s $^{(a-1)}$)	R_{ct} (Ω)
TCA75:Cz25	4587	0.6801	135 146
TCA50:Cz50	2870	0.7081	124 257
TCA25:Cz75	3102	0.7894	102 737
Cz	1570	0.7590	65 000

Conclusion

Because the electropolymerization of TCA alone by anodic oxidation proved difficult, mixtures of TCA and carbazole were investigated. Electrooxidation of these mixtures led to the formation of conductive polymer films, with higher carbazole content facilitating the polymeri- zation process, as evidenced by cyclic voltammetry. The polymerization followed an ECE mechanism involving oxidation of the peripheral carbazole units. Increasing the carbazole proportion enhances the electrochemical performance of the polymer films, resulting in higher electroactivity, greater capacitance, and lower charge-transfer resis- tance. while its morphology was granular and similar to that of polycarbazole but without cracks. Morphologically, these films exhibit a granular structure similar to polycarbazole but without cracks, which improves film homogeneity and preserves their properties. Among the studied compositions, the electrodeposited polymer film obtained from a TCA25:Cz75 electrolyte shows the best overall performance in terms of electron transfer and energy storage. Based on the observed electro- chemical properties – high electroactivity, enhanced capacitance, and low charge-transfer resistance – combined with the homogeneous granular morphology of the TCA–carbazole films, TCA-carbazole poly- mer films are particularly promising for energy storage applications,such as supercapacitors, where efficient charge transport and stable electroactive films are critical.

Acknowledgments

This work was partly supported by the French RENATECH network and its FEMTO-ST technological facility for Apreo 2 SEM im- aging and NEXSA G2 XPS analysis. This work has been achieved in the frame of the EIPHI Graduate school (contract “ANR-17-EURE-0002”).

.

References

[1] Z. Wu, Q. Zhao, X. Luo, H. Ma, W. Zheng, J. Yu, Z. Zhang, K. Zhang, K. Qu, R. Yang, N. Jian, J. Hou, X. Liu, J. Xu, B. Lu, Low-cost fabrication of high-performance fluorinated polythiophene-based vis–NIR electrochromic devices toward deformable display and camouflage, Chem. Mater. 34 (2022) 9923–9933, https:// doi.org/10.1021/acs.chemmater.2c01964.

[2] A.R. Murad, A. Iraqi, S.B. Aziz, S.N. Abdullah, M.A. Brza, Conducting polymers for optoelectronic devices and organic solar cells: a review, Polymers (Basel) 12 (2020) 2627, https://doi.org/10.3390/polym12112627.

[3] C.H. Du, Y.H. Xu, H. Li, Z.X. Wu, H.J. Yang, X.M. Liu, B.Y. Lu, G.M. Nie, G. Zhang, Tough hydrogen bonding crosslinked poly (3-fluorothiophene) network via electrosynthesis for high-performance electrochromic supercapacitors, Chin. J. Polym. Sci. 42 (2024) 1749–1757, https://doi.org/10.1007/s10118-024-3175-8.

[4] M.G. Sumdani, M.R. Islam, A.N.A. Yahaya, S.I. Safie, Recent advancements in synthesis, properties, and applications of conductive polymers for electrochemical energy storage devices: a review, Polym. Eng. Sci. 62 (2022) 269–303, https://doi. org/10.1002/pen.25859.

[5] M. Yao, Z. Wang, Z. Li, G. Li, H. Wang, J. Xu, B. Lu, Facile in-situ electrosynthesis of a novel PEDOT derivative for efficient uranium electroextraction, Sep. Purif. Technol. 365 (2025) 132432,

https://doi.org/10.1016/j.seppur.2025.132432.
[6] S. Lakard, B. Lakard, Environmental applications of conducting polymers and their composites: adsorption and detection of heavy metal ions, J. Environ. Chem. Eng. 13 (2025) 116233, https://doi.org/10.1016/j.jece.2025.116233.
[7] J.-X. Jiang, F. Su, A. Trewin, C.D. Wood, N.L. Campbell, H. Niu, C. Dickinson, A. Y. Ganin, M.J. Rosseinsky, Y.Z. Khimyak, A.I. Cooper, Conjugated microporous poly(Aryleneethynylene) networks, Angew. Chem. Int. Ed. 46 (2007) 8574–8578, https://doi.org/10.1002/anie.200701595.
[8] M. Trunk, A. Herrmann, H. Bildirir, A. Yassin, J. Schmidt, A. Thomas, Copper-free sonogashira coupling for high-surface-area conjugated microporous poly (Aryleneethynylene) networks, Chem. - Eur. J. 22 (2016) 7179–7183, https://doi. org/10.1002/chem.201600783.
[9] J.M.H. Thomas, C. Mollart, L. Turner, P. Heasman, P. Fayon, A. Trewin, Artificial synthesis of conjugated microporous polymers via Sonogashira–Hagihara coupling, J. Phys. Chem. B 124 (2020) 7318–7326, https://doi.org/10.1021/acs. jpcb.0c04850.
[10] A.F. Saber, S.U. Sharma, J.T. Lee, A.F. El-Mahdy, S.W. Kuo, Carbazole-conjugated microporous polymers from Suzuki–Miyaura coupling for supercapacitors, Polymer (Guildf) 254 (2022) 125070, https://doi.org/10.1016/j.polymer.2022.125070.
[11] D.G. Teng, X.Y. Wei, J.H. Li, H.S. Gao, M. Zhang, Z.M. Zong, One-pot facile synthesis of multifunctional conjugated microporous polymers via Suzuki-Miyaura coupling reaction, ChemistrySelect 5 (2020) 1410–1415, https://doi.org/10.1002/ slct.201904303.
[12] Z. Tan, H. Su, Y. Guo, H. Liu, B. Liao, A.M. Amin, Q. Liu, Ferrocene-based conjugated microporous polymers derived from Yamamoto coupling for gas storage and dye removal, Polymers (Basel) 12 (2020) 719, https://doi.org/ 10.3390/polym12030719.
[13] J. Schmidt, M. Werner, A. Thomas, Conjugated microporous polymer networks via Yamamoto polymerization, Macromolecules 42 (2009) 4426–4429, https://doi. org/10.1021/ma9005473.
[14] S. Luo, Z. Zeng, G. Zeng, Z. Liu, R. Xiao, P. Xu, H. Wang, D. Huang, Y. Liu, B. Shao, Q. Liang, D. Wang, Y. Fu, Recent advances in conjugated microporous polymers for photocatalysis: designs, applications, and prospects, J. Mater. Chem. A 8 (2020) 6434–6470, https://doi.org/10.1039/d0ta01102a.
[15] W. Zhang, C. Shu, H. Cui, Q. Wan, C.T. Au, B. Yi, H. Yang, Carbazolic conjugated microporous polymers for photocatalytic organic transformations, Macromol. Rapid Commun. 44 (2023) 2300012, https://doi.org/10.1002/marc.202300012.
[16] K. Amin, N. Ashraf, L. Mao, C.F. Faul, Z. Wei, Conjugated microporous polymers for energy storage: recent progress and challenges, Nano Energy 85 (2021) 105958, https://doi.org/10.1016/j.nanoen.2021.105958.
[17] T.H. Weng, M.G. Mohamed, S.U. Sharma, S.V. Chaganti, M.M. Samy, J.T. Lee, S. W. Kuo, Ultrastable three-dimensional triptycene-and tetraphenylethene- conjugated microporous polymers for energy storage, ACS Appl. Energy Mater. 5 (2022) 14239–14249, https://doi.org/10.1021/acsaem.2c02809.
[18] X. Sheng, H. Shi, L. Yang, P. Shao, K. Yu, X. Luo, Rationally designed conjugated microporous polymers for contaminants adsorption, Sci. Total Environ. 750 (2021) 141683, https://doi.org/10.1016/j.scitotenv.2020.141683.
[19] N. Wan, Q. Chang, F. Hou, S. Zhang, X. Zang, X. Zhao, C. Wang, Z. Wang, Y. Yamauchi, Nanoarchitectured conjugated microporous polymers: state of the art synthetic strategies and opportunities for adsorption science, Chem. Mater. 34 (2022) 7598–7619, https://doi.org/10.1021/acs.chemmater.2c00999.
[20] F. Piron, P. Leriche, G. Mabon, I. Grosu, J. Roncali, Electropolymerization of three- dimensional π-conjugated system based on 3, 4-ethylenedioxythiophene (EDOT), Electrochem. Commun. 10 (2008) 1427–1430, https://doi.org/10.1016/j. elecom.2008.07.014.

[21] F. Piron, P. Leriche, I. Grosu, J. Roncali, Electropolymerizable 3D π-conjugated architectures with ethylenedioxythiophene (EDOT) end-groups as precursors of electroactive conjugated networks, J. Mater. Chem. 20 (2010) 10260–10268, https://doi.org/10.1039/c0jm01873b.
[22] C. Gu, Y. Chen, Z. Zhang, S. Xue, S. Sun, K. Zhang, C. Zhong, H. Zhang, Y. Pan, Y. Lv, F. Li, S. Zhang, F. Huang, Y. Ma, Electrochemical route to fabricate film-like conjugated microporous polymers and application for organic electronics, Adv. Mater. 25 (2013) 3443–3448, https://doi.org/10.1002/adma.201300839.
[23] C. Gu, N. Huang, J. Gao, F. Xu, Y. Xu, D. Jiang, Controlled synthesis of conjugated microporous polymer films: versatile platforms for highly sensitive and label-free chemo-and biosensing, Angew. Chem. Int. Ed. 53 (2014) 4850–4855, https://doi. org/10.1002/anie.201402141.
[24] M. Ates, N. Uludag, Carbazole derivative synthesis and their electropolymerization, J. Solid State Electrochem. 20 (2016) 2599–2612, https://doi.org/10.1007/ s10008-016-3269-5.
[25] F. Bekkar, F. Bettahar, I. Moreno, R. Meghabar, M. Hamadouche, E. Hernáez, J. L. Vilas-Vilela, L. Ruiz-Rubio, Polycarbazole and its derivatives: synthesis and applications. a review of the last 10 years, Polymers (Basel) 12 (2020) 2227, https://doi.org/10.3390/polym12102227.
[26] E. Contal, C.M. Sougueh, S. Lakard, A. Et Taouil, C. Magnenet, B. Lakard, Investigation of polycarbazoles thin films prepared by electrochemical oxidation of synthesized carbazole derivatives, Front. Mater. 6 (2019) 131, https://doi.org/ 10.3389/fmats.2019.00131.
[27] J.H. Scofield, Hartree-Slater Subshell photoionization cross-sections at 1254 and 1487 eV, J. Electron Spectrosc. Relat. Phenom. 8 (1976) 129–137, https://doi.org/ 10.1016/0368-2048(76)80015-1.
[28] K. Pithaksinsakul, T. Burton, C. Pareseecharoen, S. Deebansok, V. Promarak, O. Fontaine, Novel carbazole-based ionic liquids and their charge-transfer kinetics pertaining to Marcus theory towards highly efficient redox active electrolytes, New J. Chem. 48 (2024) 2439–2447, https://doi.org/10.1039/d3nj02760k.
[29] G. Bagdžiu nas, D. Palinauskas, Poly (9 H-carbazole) as a organic semiconductor for enzymatic and non-enzymatic glucose sensors, Biosensors (Basel) 10 (2020) 104, https://doi.org/10.3390/bios10090104.
[30] S. Lakard, E. Contal, K. Mougin, C. Magnenet, B. Lakard, Electrochemical preparation and physicochemical study of polymers obtained from carbazole and N-((methoxycarbonyl) methyl) carbazole, Synth. Met. 270 (2020) 116584, https:// doi.org/10.1016/j.synthmet.2020.116584.
[31] S. Lakard, E. Contal, K. Mougin, B. Lakard, Electrodeposition and characterization of conducting polymer films obtained from carbazole and 2-(9H-carbazol-9-yl) acetic acid, Electrochem 3 (2022) 322–336, https://doi.org/10.3390/ electrochem3020022.
[32] J.F. Ambrose, R.F. Nelson, Anodic oxidation pathways of carbazoles: I. carbazole and N-substituted derivatives, J. Electrochem. Soc. 115 (1968) 1159, https://doi.org/10.1149/1.2410929jes.
[33] E. Contal, S. Lakard, F. Dumur, B. Lakard, Investigation of polycarbazoles thin films prepared by electrochemical oxidation of 3- and 9-substituted carbazoles, Prog. Org. Coat. 162 (2022) 106563, https://doi.org/10.1016/j.porgcoat.2021.106563.
[34] A.A. Kocaeren, D.Ş. Bahçeci, B. Kizilkaya, F. Doğan, Electrochemical polymer synthesis using thiophene and pyrrole/carbazole: their electrochemical behaviours and capacitor performance, J. Electroanal. Chem. (2024) 118486, https://doi.org/10.1016/j.jelechem.2024.118486.
[35] C.W. Kuo, J.K. Chang, Y.C. Lin, T.Y. Wu, P.Y. Lee, T.H. Ho, Poly(tris (4-carbazoyl- 9-ylphenyl) amine) /three poly (3, 4-ethylenedioxythiophene) derivatives in complementary high-contrast electrochromic devices, Polymers (Basel) 9 (2017) 543, https://doi.org/10.3390/polym9100543.

[36] J. Kimpel, Y. Yoshitake, T. Michinobu, Poly(3,9-carbazole)s: a chemically stable extended form of polyaniline for nitro-aromatic sensor applications, Bull. Chem. Soc. Jpn 193 (2020) 361–1365, https://doi.org/10.1246/bcsj.20200177.
[37] H. Jiang, L. Yang, C. Li, C. Yan, P.S. Lee, J. Ma, High–rate electrochemical capacitors from highly graphitic carbon–tipped manganese oxide/mesoporous carbon/manganese oxide hybrid nanowires, Energy Environ. Sci. 4 (2011) 1813–1819, https://doi.org/10.1039/c1ee01032h.
[38] A. Aynaou, B. Youbi, M. Ait Himi, Y. Lghazi, J. Bahar, C. El Haimer, A. Ouedrhiri, I. Bimaghra, Electropolymerization investigation of polyaniline films on ITO substrate, Mater. Today Proc. 66 (2022) 335–340, https://doi.org/10.1016/j. matpr.2022.05.437.
[39] A. Kayishaer, C. Magnenet, I.A. Pavel, H.B. Halima, V. Moutarlier, B. Lakard, N. Redon, C. Duc, S. Lakard, Influence of surfactant on conductivity, capacitance and doping of electrodeposited polyaniline films, Front. Mater. 11 (2024) 1358534, https://doi.org/10.3389/fmats.2024.1358534.
[40] Y. Xie, J. Xu, L. Lu, C. Xia, Electrochemical investigation of lithium perchlorate- doped polypyrrole growing on titanium substrate, Inorganics 12 (2024) 125, https://doi.org/10.3390/inorganics12040125.
[41] J.R. Aggas, W. Harrell, J. Lutkenhaus, A. Guiseppi-Elie, Metal–polymer interface influences apparent electrical properties of nano-structured polyaniline films, Nanoscale 10 (2018) 672–682, https://doi.org/10.1039/c7nr06503e.
[42] C. Xing, Z. Zhang, L. Yu, L. Zhang, G.A. Bowmaker, Electrochemical corrosion behavior of carbon steel coated by polyaniline copolymers micro/nanostructures, RSC Adv. 4 (2014) 32718–32725, https://doi.org/10.1039/c4ra05826g.